Microscopic in-medium nucleon-nucleon cross sections with improved Pauli blocking effects for applications in nuclear reactions

A Thesis

Presented in Partial Fulfilment of the Requirements for the

Degree of Master of Science

with a

Major in Physics

in the

College of Graduate Studies

University of Idaho

by

Boyu Chen

May 2014

Major Professor: Francesca Sammarruca, Ph.D.

Authorization to Submit Thesis

This thesis of Boyu Chen, submitted for the degree of Master of Science with a major in Physics and titled "Microscopic in-medium nucleon-nucleon cross sections with improved Pauli blocking effects and their applications in nuclear reactions" has been reviewed in final form. Permission, as indicated by the signatures and dates given below, is now granted to submit final copies to the College of Graduate Studies for approval.

Major Professor ______________________ Date 4/29/14
Francesca Sammarruca, Ph.D.

Committee Members ______________________ Date 4/29/2014
Ruprecht Machleidt, Ph.D.

______________________ Date 4/29/2014
Robert Rinker, Ph.D.

Department Administrator ______________________ Date 4/29/14
David McIlroy, Ph.D.

Discipline's College Dean ______________________ Date 5/2/14
Paul Joyce, Ph.D.

Final Approval and Acceptance by the College of Graduate Studies

______________________ Date ______________
Jie Chen, Ph.D.

Abstract

In this thesis, we will be concerned with the development of nucleon-nucleon cross sections appropriate for scattering of two nucleons in the nuclear medium and intended for applications in nuclear reactions. In particular, we will present an improved description of the Pauli blocking mechanism. The latter is an important effect which impacts the dynamics of two fermions in the many-body systems by preventing scattering into occupied states.

A novel characteristic of the present approach combines microscopic medium effects on the scattering amplitude with a Pauli blocking mechanism which is more appropriate for applications in ion-ion reaction models as compared to a previous approach. The effective in-medium cross section is found to be quite sensitive to the description of Pauli blocking in the final configurations. Work in progress and future plans are briefly discussed.

Acknowledgements

I would like to thank my professor Francesca Samarruca for her assistance on this project. Her clear explanations and careful analysis made it possible for me to complete this master's project. I greatly appreciate everything she has done for me at the University of Idaho.

I would also like to thank Dr. Bertulani for providing us with his program to calculate knockout reactions. In addition, I would like to thank the U.S. Department of Energy for sponsoring this research, and the two other members of my thesis commitee, Dr. Rupert Machliedt and Dr. Robert Rinker.

Table of Contents

List of Figures

Chapter 1

Introduction

The investigation of the effective nucleon-nucleon (NN) interaction in dense hadronic matter is a topic of fundamental importance for nuclear reactions at intermediate energies (20 MeV/nucleon $\lesssim E_{lab} \lesssim$ 300 MeV/nucleon, where E_{lab} is the incident kinetic energy in the laboratory system) and for nuclear structure in general. The relevant literature is very vast. Reference [1] is just a representative example of the traditional microscopic approach where two-nucleon correlations in nuclear systems are introduced through the G-matrix (which is the scattering matrix in the medium). Moreover, the effective NN interaction is the main ingredient of microscopic predictions of the nuclear equation of state (EoS) and thus impacts the properties of compact stars. Dense hadronic matter can also be created in the laboratory in energetic heavy-ion (HI) collisions. Simulations of HI collisions are typically based on transport equations and describe the evolution of a non-equilibrium system of strongly interacting hadrons undergoing two-body collisions in the presence of a mean field. The Boltzmann-Uehling-Uhlenbeck equation [2, 3] and quantum molecular dynamics [4], along with their relativistic counterparts [5, 6, 7], have been typically employed to describe intermediate-energy HI reactions. *In-medium* two-body cross sections are an important component of such simulations.

In direct reactions at intermediate energies, the NN cross sections are often used as input to obtain quantum refractive and diffractive effects, replacing the role of optical potentials commonly used in low energy reactions [8]. Examples such as knockout (stripping and diffraction dissociation) reactions, elastic scattering, charge-exchange, and excitation of giant resonances, are often carried out using reaction mechanisms based on the construction of scattering matrices built from the underlying NN scattering amplitude. Reaction calculations at intermediate to high energy are often conducted within the framework of the Glauber approximation [9] and have been a frequent tool for testing nuclear models and constraining nuclear sizes. In fact, the description of complex nuclear reactions at intermediate energies based on individual NN collisions has a long tradition. In the framework of the Glauber model, the reaction cross section is written in terms of the "thickness function", which is the product of the averaged NN cross section and the overlap integral of the target and projectile local densities.

In-medium NN cross sections have been calculated with a variety of methods. In semi-phenomenological approaches, one makes the assumption that the transition matrix in the medium is approximately the same as the one in vacuum and that medium effects come in only through the use of effective masses in the phase space factor [10, 11, 12]. Then, the in-medium cross section is scaled (relative to its value in vacuum) as the square of the ratio of the (reduced) masses. Phenomenological formulas, such as the one in Ref. [13], have been developed for practical purposes and combine the energy dependence of empirical free-space NN cross sections with the density dependence of some microscopic models.

Microscopic predictions based on a medium-modified collision matrix were reported, for instance, in Ref. [14], where Dirac-Brueckner-Hartree-Fock (DBHF) medium effects were applied to obtain a medium-modified K-matrix. More recent microscopic calculations applied DBHF medium effects to produce a complex G-matrix including consideration of isospin dependence in asymmetric nuclear matter [15].

It is the purpose of this thesis to present our updated predictions of microscopic in-medium elastic NN cross sections with a more complete description of Pauli blocking. The main objective is to produce two-body cross sections which include, microscopically, all important medium effects and are suitable for realistic applications in nucleus-nucleus scattering at intermediate energies including direct and central collisions. We start from a one-boson-exchange NN potential, which describes well the elastic part of the NN interaction up to high energy. Thus, as long as we are not interested in pion production, which is negligible up to, at least, several hundreds of MeV, it is reasonable to use NN elastic cross sections as input to the reaction model. Of course, the elastic part of the NN interaction can and does generate inelastic nucleus-nucleus scattering.

In Chapter 2, we describe the details of the calculation and highlight the differences with our previous approach. We then present a selection of results (Chapter 3). Since calculations of the microscopic and Pauli-blocked cross sections are lengthy and computationally time consuming, we develop a convenient parametrization as a function of projectile and target densities and incident energy. This effort is described in Chapter 4. A summary and conclusive remarks are contained in Chapter 5.

Chapter 2

Geometric Pauli blocking and the average in-medium NN cross section

2.1 The average in-medium NN cross section

The average cross section for scattering of two Fermi spheres with relative momentum k, see Fig. 2.1, is given by [16]:

$$\bar{\sigma}_{NN} = \frac{1}{V_{F1}V_{F2}} \int_{V_{F1}} \int_{V_{F2}} d\mathbf{k}_1 d\mathbf{k}_2 \sigma^{NN}_{Pauli}(\mathbf{q}, \mathbf{q}^{'}) \ , \tag{2.1}$$

where V_{F1} and V_{F2} are the volumes of the Fermi spheres and σ^{NN}_{Pauli} is the (Pauli-restricted) cross section for scattering of two nucleons within the Fermi spheres. The variable $\mathbf{q} = (\mathbf{k}_1 - \mathbf{k}_2 + \mathbf{k})/2$ and $\mathbf{q}^{'} = (\mathbf{k}_1^{'} - \mathbf{k}_2^{'} + \mathbf{k})/2$ are relative momenta before and after collision, respectively, with $|\mathbf{q}| = |\mathbf{q}^{'}|$. The nucleon-nucleon cross section, σ^{NN}, is defined with reference to a typical NN scattering experiment, with the target nucleon at rest and the incoming nucleon having momentum $k = 2q$, whereas in our scenario all relative momenta off the symmetry axis of the two Fermi spheres are considered, see Fig. 2.1. For this reason, a correction factor, $2q/k$, is inserted in Eq. (2.1), which is then written as [16]

$$\bar{\sigma}_{NN} = \frac{1}{V_{F1}V_{F2}} \int_{V_{F1}} \int_{V_{F2}} d\mathbf{k}_1 d\mathbf{k}_2 \frac{2q}{k} \sigma^{NN}_{Pauli}(q). \tag{2.2}$$

Note that, with the approximation $2q = k$, the total effective cross section would be defined as

$$\bar{\sigma}_{NN} = \int \frac{d\sigma^{NN}_{Pauli}(q)}{d\Omega} d\,\Omega \ , \tag{2.3}$$

or, assuming space isotropy of the differential cross section,

$$\bar{\sigma}_{NN} = \frac{\sigma^{NN}_{Pauli}(q)}{4\pi} \int d\Omega \ , \tag{2.4}$$

which is consistent with Eq. (2.2) if $2q = k$.

When expressed in terms of differential cross section, Eq. (2.2) takes the following form:

$$\bar{\sigma}_{NN} = \frac{1}{V_{F1}V_{F2}} \int_{V_{F1}} \int_{V_{F2}} d\mathbf{k}_1 d\mathbf{k}_2 \frac{2q}{k} \int_{all\ angles} \frac{d\sigma^{NN}_{Pauli}(q)}{d\Omega} d\Omega \ . \tag{2.5}$$

Pauli blocking restrictions on σ^{NN}_{Pauli} requires

$$\sigma^{NN}_{Pauli}(q) = \begin{cases} \sigma^{NN}_{T}(q) & \text{if } |\mathbf{k}'_1| > k_{F1},\ |\mathbf{k}'_2| > k_{F2} \\ 0 & \text{otherwise,} \end{cases} \tag{2.6}$$

where σ^{NN}_T is often taken as the empirical free-space NN cross section. Transfering the Pauli blocking restriction from σ^{NN}_{Pauli} to the solid-angle, the integral in Eq. (2.5) becomes

$$\bar{\sigma}_{NN} = \frac{1}{V_{F1}V_{F2}} \int_{V_{F1}} \int_{V_{F2}} d\mathbf{k}_1 d\mathbf{k}_2 \frac{2q}{k} \int_{Pauli} \frac{d\sigma^{NN}_{T}(q)}{d\Omega} d\Omega \ , \tag{2.7}$$

where *pauli* stands for the Pauli-allowed angles. Assuming $\frac{d\sigma^{NN}_T(q)}{d\Omega} = \frac{\sigma^{NN}_T(q)}{4\pi}$, we have

$$\bar{\sigma}_{NN}(k, k_{F1}, k_{F2}) = \frac{1}{V_{F1}V_{F2}} \int_{V_{F1}} \int_{V_{F2}} d\mathbf{k}_1 d\mathbf{k}_2 \frac{2q}{k} \frac{\sigma^{NN}_{T}(q)}{4\pi} \int_{Pauli} d\Omega \ . \tag{2.8}$$

Typically, some free-space parametrization of the free-space NN cross sections is employed for σ^{NN}_T. In our case, though, the input of Eq. (2.8) are microscopic effective NN cross sections obtained within the Dirac-Brueckner-Hartree-Fock (DBHF) scheme. They contain additional medium effects arising from the presence of the nuclear matter potential and Pauli blocking of the intermediate states (see Ref. [17, 18] for details).

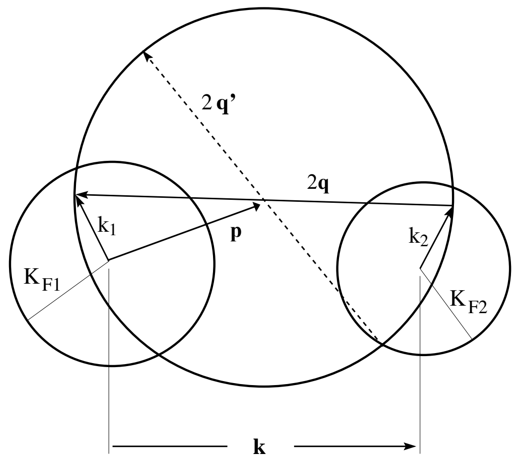

Figure 2.1: Geometrical representation of Pauli blocking.

2.2 Derivation of the Pauli-allowed solid angle

In the calculation of the integral $\int_{Pauli} d\Omega$, one employs geometrical arguments schematically represented in Fig. 2.1, where the two Fermi spheres represent the densities of the target and projectile nuclei. Note that $\mathbf{k_1}$ and $\mathbf{k_2}+\mathbf{k}$ are the momenta of the two nucleons with respect to the same point. Then, the relative momentum $2\mathbf{q}$ and the total momentum $2\mathbf{p}$ are given by $2\mathbf{q} = \mathbf{k}_2 + \mathbf{k} - \mathbf{k}_1$, and $2\mathbf{p} = \mathbf{k}_1 + \mathbf{k}_2 + \mathbf{k}$, respectively. The larger circle in the figure is centered at $\mathbf{p}$ while $|\mathbf{q}|$ is the radius of the scattering sphere. The vector $2\mathbf{q}$ can rotate around the scattering sphere while maintaining constant magnitude due to energy-momentum conservation.

We highlight that, with the definitions given above, relative momenta off the symmetry axis of the two Fermi spheres (the $\mathbf{k}$ direction) are allowed, which is not the case with assumptions we made previously [15], where we defined, for simplicity, $\mathbf{q} = \mathbf{p} = \mathbf{k}/2$. With the present definitions, instead, we average momenta of the two interacting nucleons in arbitrary directions. In turn, this impacts the solid angle allowed by Pauli blocking, as shown below.

It is also convenient to define the momentum $2\mathbf{b} = \mathbf{k_2} + \mathbf{k_1} - \mathbf{k}$. Assuming the

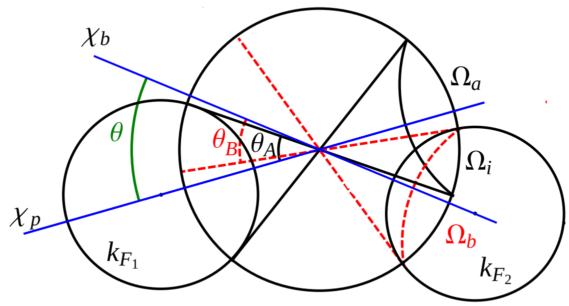

Figure 2.2: Two-dimensional projection of the geomerty of Pauli blocking.

collision is elastic, conservation of energy and momentum requires

$$\begin{aligned} 2\mathbf{p} &= \mathbf{k_1'} + \mathbf{k_2'} + \mathbf{k} \\ 2\mathbf{q}' &= \mathbf{k_2'} - \mathbf{k_1'} + \mathbf{k} \\ 2\mathbf{b} &= \mathbf{k_1'} + \mathbf{k_2'} - \mathbf{k}\ . \end{aligned} \tag{2.9}$$

The quantities $\mathbf{k_1'}$ and $\mathbf{k_2'}$ are the momenta of two nucleons after the collision, whereas $\mathbf{q}'$ is the relative momentum after collision, with $|\mathbf{q}'| = |\mathbf{q}|$. Because of the Pauli exclusion principle, the following restrictions apply:

$$\begin{aligned} |\mathbf{k_1'}| &= |\mathbf{p} - \mathbf{q}'| > k_{F1} \\ |\mathbf{k_2'}| &= |\mathbf{b} + \mathbf{q}'| > k_{F2}\ , \end{aligned} \tag{2.10}$$

or,

$$\begin{aligned} p^2 + q^2 - 2pq\cos\alpha_1 &> k_{F1}^2 \\ b^2 + q^2 + 2bq\cos\alpha_2 &> k_{F2}^2\ . \end{aligned} \tag{2.11}$$

In the equations above, α_1 is the angle between $\mathbf{p}$ and $\mathbf{q}'$, and α_2 the angle between $\mathbf{b}$ and $\mathbf{q}'$. As illustrated in Fig. 2.2, we have

$$\begin{aligned} \cos\theta_A &= \tfrac{p^2+q^2-k_{F1}^2}{2pq} \\ \cos\theta_B &= \tfrac{b^2+q^2-k_{F2}^2}{2bq}\ , \end{aligned} \tag{2.12}$$

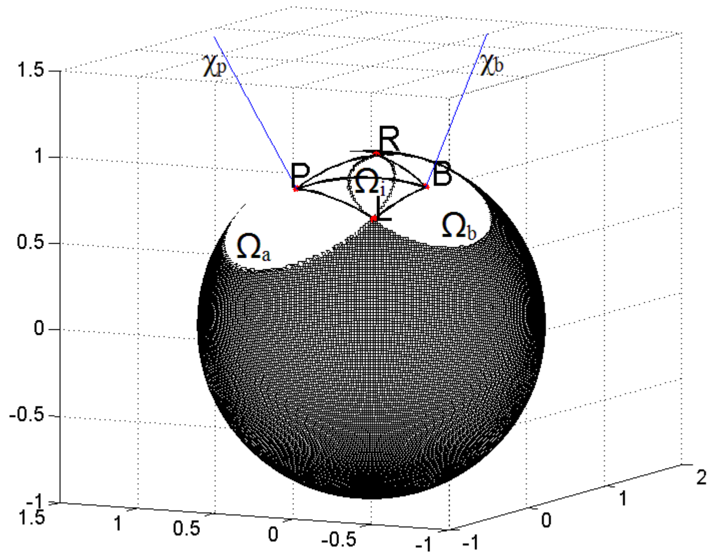

Figure 2.3: Pauli blocking of two nucleons in three dimension.

with θ_A and θ_B are the excluded polar angles. The excluded solid angles for each nucleon are then given by

$$\begin{aligned} \Omega_a &= 2\pi(1-\cos\theta_A) \\ \Omega_b &= 2\pi(1-\cos\theta_B)\ , \end{aligned} \tag{2.13}$$

and therefore the total allowed solid angle can be obtained from

$$\Omega_{pauli} = 4\pi - 2(\Omega_a + \Omega_b - \bar{\Omega})\ , \tag{2.14}$$

where $\bar{\Omega}$ represents the intersection of the two conical sections Ω_a and Ω_b. The full calculation has already been done in Ref. [19]; however, in here we will use a slightly different approach to calculate $\bar{\Omega}$. Fig. 2.3 shows how Ω_a and Ω_b are projected on the surface of a unit sphere. If Ω_i is the intersection of Ω_a and Ω_b, it is obvious that

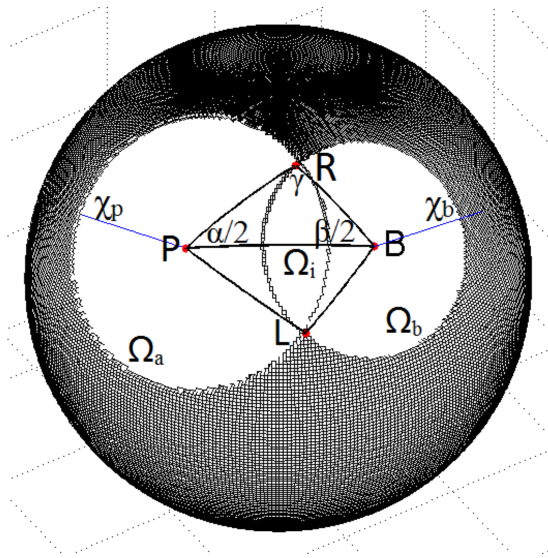

Figure 2.4: A different view of Pauli blocking of two nucleons in three dimension.

$$\Omega_i = \begin{cases} 0 & \text{if } \theta > \theta_A + \theta_B; \\ \Omega_b & \text{if } \theta_B < \theta_A, \theta < |\theta_B - \theta_A|; \\ \Omega_a & \text{if } \theta_A < \theta_B, \theta < |\theta_B - \theta_A|. \end{cases} \tag{2.15}$$

The case $|\theta_B - \theta_A| < \theta < \theta_A + \theta_B$ is more complex than the other three cases and a more detailed study is needed. As shown in Fig. 2.4, P and B are the centers of the two circular projections Ω_a and Ω_b. The two circular contours intersect at R and L. $\alpha/2$, $\beta/2$ and γ are the internal angles of the spherical triangle PBR. The circular sectors of Ω_a and Ω_b have areas equal to $\frac{\alpha}{2\pi}\Omega_a$ and $\frac{\beta}{2\pi}\Omega_b$, respectively. Apparently, the intersection area of Ω_a and Ω_b is given by

$$\Omega_i = \frac{\alpha}{2\pi}\Omega_a + \frac{\beta}{2\pi}\Omega_b - 2\Delta_{PRB} \ . \tag{2.16}$$

Here, Δ_{PRB} is the area of the spherical triangle PBR. To obtain $\alpha/2$, first we define the center of the unit sphere, O, as the orgin of the system, and χ_p along the z-axis. Point B is at location $(1, \theta, \alpha/2)$, while point L has coordinates $(1, \theta_A, 0)$. We can then write:

$$\mathbf{OB} \cdot \mathbf{OL} = \cos\theta_B = \cos\theta_A \cos\theta + \sin\theta_A \sin\theta \cos(\alpha/2) \;, \tag{2.17}$$

from which $\alpha/2$ can be readily obtained as

$$\alpha/2 = \arccos(\frac{\cos\theta_B - \cos\theta\cos\theta_A}{\sin\theta\sin\theta_A}) \;. \tag{2.18}$$

In a similar fashion we find $\beta/2$ to be given by

$$\beta/2 = \arccos(\frac{\cos\theta_A - \cos\theta\cos\theta_B}{\sin\theta\sin\theta_B}) \;. \tag{2.19}$$

Applying the law of cosines of spherical trigonometry,

$$\cos\gamma = -\cos(\alpha/2)\cos(\beta/2) + \sin(\alpha/2)\sin(\beta/2)\cos\theta \;, \tag{2.20}$$

we obtain

$$\gamma = \arccos[-\cos(\alpha/2)\cos(\beta/2) + \sin(\alpha/2)\sin(\beta/2)\cos\theta] \;. \tag{2.21}$$

From Girard's theorem of spherical trigonometry, we have

$$\Delta_{PRB} = \alpha/2 + \beta/2 + \gamma - \pi \;. \tag{2.22}$$

Inserting Eq. (2.21) and Eq. (2.22) into Eq. (2.16), the solid angle Ω_i is found to have the following value

$$\Omega_i = 2\{\pi - \cos\theta_A \cos^{-1}(\delta_{AB}) - \cos\theta_B \cos^{-1}(\delta_{BA}) - \cos^{-1}[\cos\theta\sqrt{(1-\delta_{AB}^2)(1-\delta_{BA}^2)} - \delta_{AB}\delta_{BA}]\} \;, \tag{2.23}$$

where

$$\delta_{ij} = \frac{\cos\theta_i - \cos\theta\cos\theta_j}{\sin\theta\sin\theta_j}\ . \tag{2.24}$$

Noticing that, while $\theta + \theta_A + \theta_B > \pi$, Ω_a and Ω_b have two intersections on the hemisphere, we have

$$\bar{\Omega} = \Omega_i(\theta, \theta_A, \theta_B) + \Omega_i(\pi - \theta, \theta_A, \theta_B)\ . \tag{2.25}$$

Chapter 3

Predictions for in-medium NN cross sections and preliminary applications

3.1 Discussion of our predictions

As pointed out in Chapter 2, particularly with regard to Eq. (2.8), the properly averaged and geometrically Pauli blocked in-medium cross section can be written as

$$\bar{\sigma}_{NN}(k, k_{F1}, k_{F2}) = \frac{1}{V_{F1}V_{F2}} \int_{V_{F1}} \int_{V_{F2}} d\mathbf{k}_1 d\mathbf{k}_2 \frac{2q}{k} \frac{\sigma_{DBHF}(q)}{4\pi} \int_{Pauli} d\Omega \ , \tag{3.1}$$

where, in our case, $\sigma_T^{NN}(q) = \sigma_{DBHF}(q)$ is the (microscopic) NN cross section which contains additional medium effects, see comments made on p.5 following Eq. (2.8).

In order to highlight the differences between the in-medium cross section, $\sigma_{DBHF}(q)$, and the *averaged* effective cross section, $\bar{\sigma}_{NN}(k, k_{F1}, k_{F2})$, we begin by showing just the input of Eq. (3.1), $\sigma_{DBHF}(q)$, for *pp* scattering (Fig. 3.1) and for *np* scattering (Fig. 3.2), as a function of the two-nucleon relative momentum q. On the left, we display a variety of cases where the two Fermi spheres have equal radii (that is, equal Fermi momenta), whereas asymmetric cases are shown on the right.

The cross sections shown in Figs. 3.1-3.2 are just a baseline, as the important mechanism of geometric Pauli blocking of the final momenta is not yet taken into account. When such effect is applied through Eq. (3.1), the outcome is dramatically different, as is to be expected. This is displayed in Figs. 3.3-3.4 for *pp* and *np* scattering, respectively. After "overcoming" complete Pauli blocking, the cross section generally rises with increasing incident momentum. In the *np* case, we observe, at least at the lower densities, a broad maximum. In all cases, the cross sections become nearly flat at the larger momenta.

To explore the model dependence of these effective cross sections, In Figs. 3.5-3.6, we show a similar study as the one displayed in Figs. 3.1-3.2, but for the microscopic

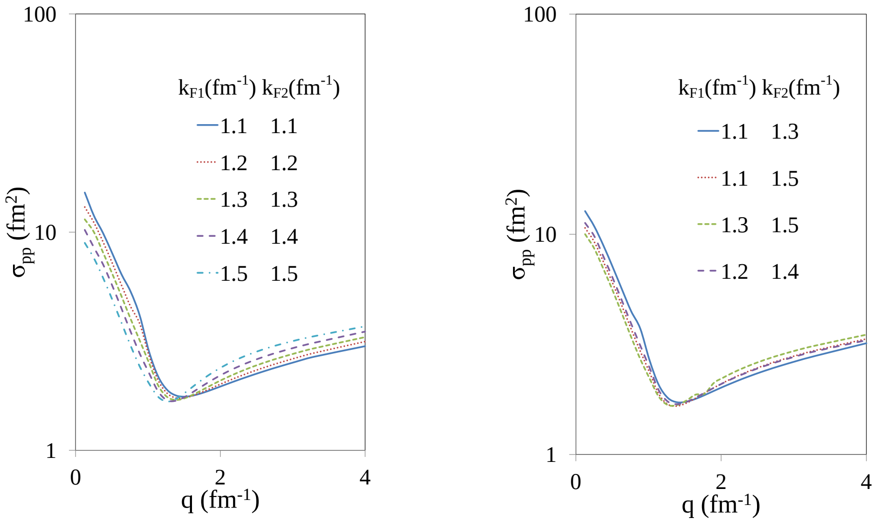

Figure 3.1: In-medium *pp* cross sections predicted by our DBHF approach for a variety of symmetric ($k_{F1} = k_{F2}$) and asymmetric ($k_{F1} \neq k_{F2}$) situations.

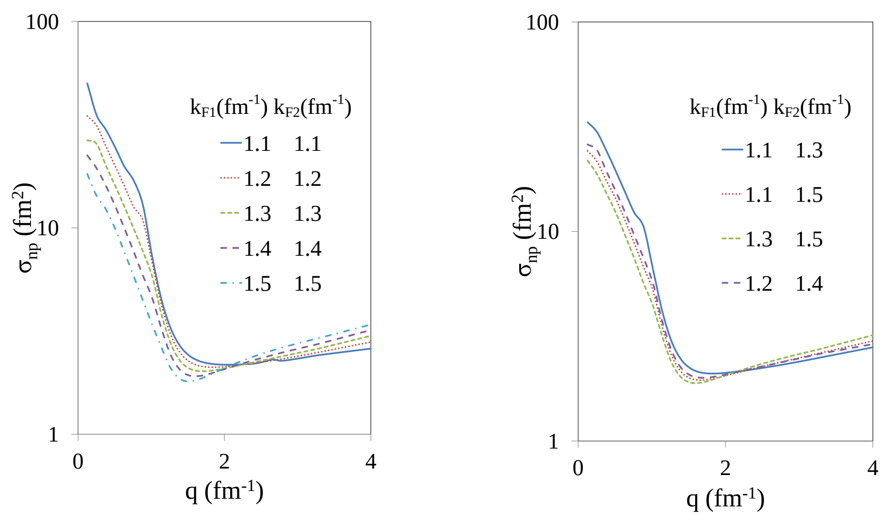

Figure 3.2: As in Fig. 3.1 for *np* scattering.

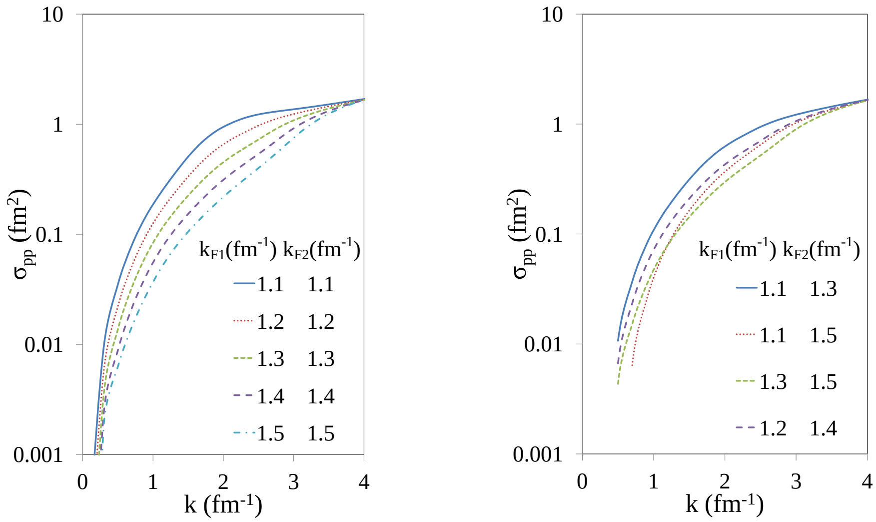

Figure 3.3: Average in-medium pp cross sections calculated as in Eq. (3.1) for a variety of symmetric ($k_{F1} = k_{F2}$) and asymmetric ($k_{F1} \neq k_{F2}$) situations.

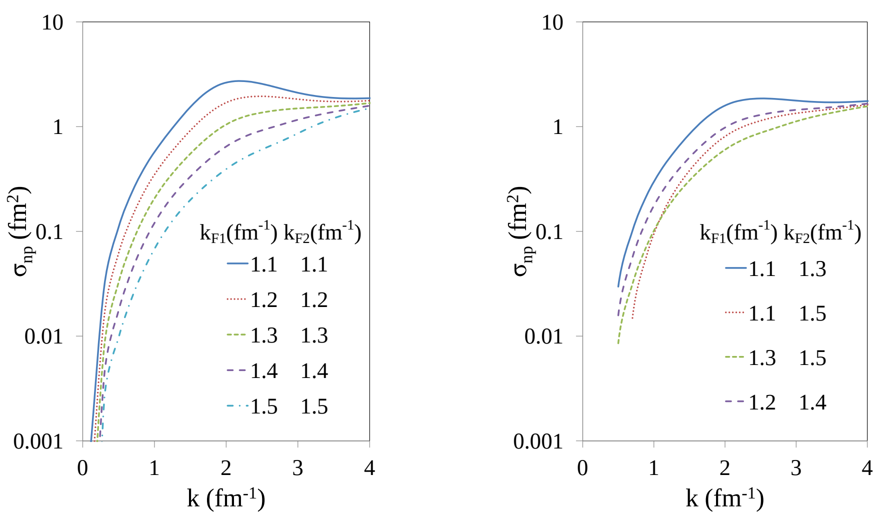

Figure 3.4: As in Fig. 3.3 for np scattering.

in-medium cross sections of Ref. [14], which are based on DBHF medium modifications of the (real) scattering K-matrix in symmetric nuclear matter, whereas we construct our in-medium cross sections from the (complex) G-matrix in asymmetric nuclear matter. Convenient parametrizations of the actual predictions from Ref. [14] as a function of energy and density are provided in the same paper, and we will use those for the present comparison. In what follows, we refer to such parametrization as the "L.&M. formula". By comparing Figs. 3.1-3.2 and Figs. 3.5-3.6 we observe that the two sets of predictions, namely the dashed curves (our calculations) and the solid curves (from Ref. [14]), have a qualitatively similar structure at the lower momenta, whereas, at the higher momenta, the predictions from the LM formula rise steeply with increasing momenta. Most likely, though, the LM formula is valid within a limited range of incident laboratory energies, about 300 MeV, which corresponds to a value of q of just below 2 fm^{-1}.

In Figs. 3.7-3.8, we show the result of using the LM formula in Eq. (3.1) (solid curves), in comparison with our predictions, already displayed in Figs. 3.3-3.4 (dashed curves). We observe that, from Eq. (3.1), larger momenta give the largest contribution to the average cross section (as the lower momenta are more strongly suppressed by geometric Pauli blocking). Therefore, the result of applying Eq. (3.1) using the LM formula as input produces larger values of the average cross section, due to the much larger values of the integrand at high q, see Figs. 3.5. In view of the comments made above with regard to the limited validity of the LM formula, caution must be exercised when applying this parametrization over a large range of momenta (as may be required by Eq. (3.1)).

From the observations made in this Chapter, we conclude that there is large model dependence among predictions of in-medium NN cross sections, which can be expected to impact corresponding predictions of (directly observable) reaction cross sections.

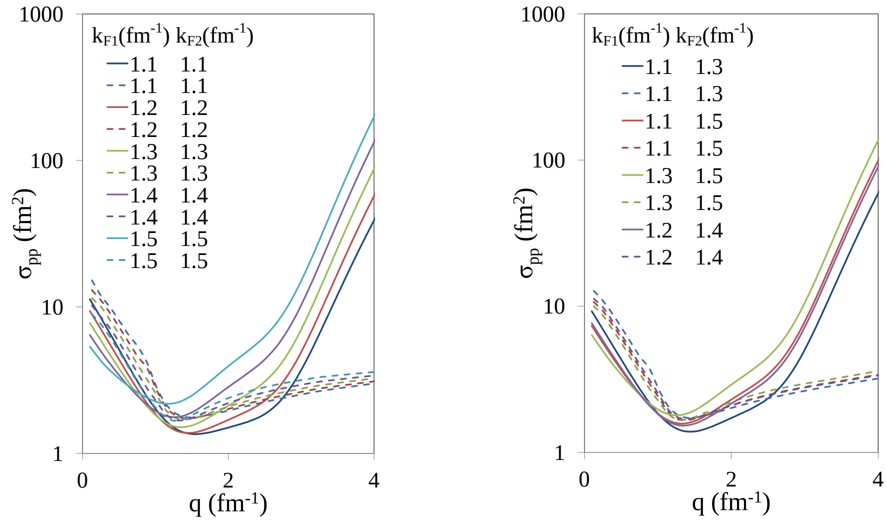

Figure 3.5: In-medium pp cross section predicted with the LM formula (solid curves) and our DBHF approach (dashed curves) for a variety of symmetric ($k_{F1} = k_{F2}$) and asymmetric ($k_{F1} \neq k_{F2}$) situations.

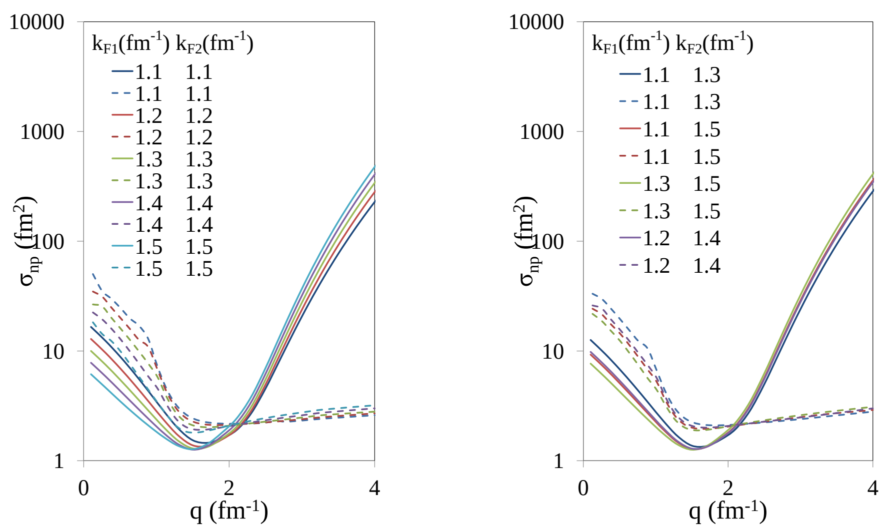

Figure 3.6: As in Fig. 3.5 for np scattering.

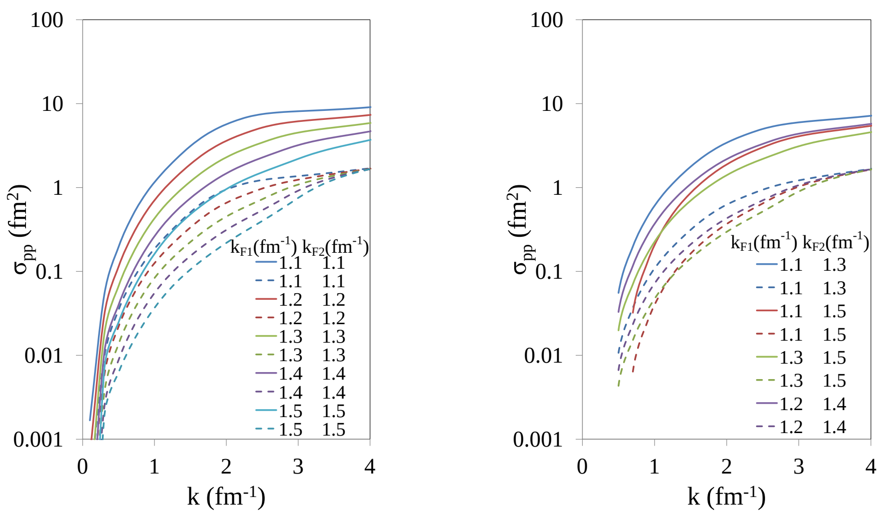

Figure 3.7: Average in-medium pp cross section for a variety of symmetric ($k_{F1} = k_{F2}$) and asymmetric ($k_{F1} \neq k_{F2}$) situations. Solid curves: predictions obtained with the LM formula (see text for details) in the integrand of Eq. (2.8); dashed curves: predictions as in Fig. 3.3.

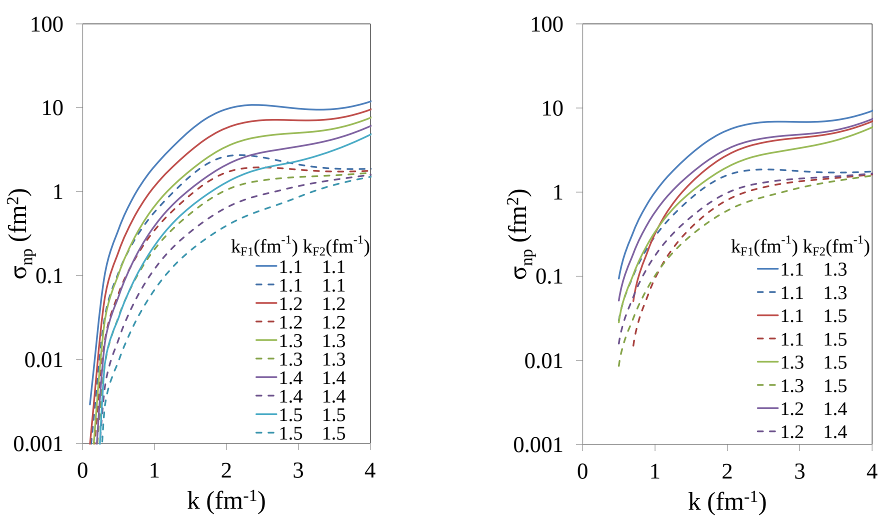

Figure 3.8: As in Fig. 3.7 for np scattering.

3.2 Plans for future applications and sensitivity tests

Our future plans include applications of the in-medium cross sections shown in the previous section to nucleus-nucleus reactions. Although systematic applications are beyond the scopes of this thesis, in this section we will set the foundations for future work and perform some exploratory reaction calculations.

Of particular interest to us will be the so-called *knockout* reactions at intermediate energies. Schematically, the process can be described as

$$(c + N) + T \rightarrow c + X \ , \tag{3.2}$$

where the projectile, typically, consists of a core, c and a valence nucleon, N, and T is the target, usually a light ion. The scattering causes the removal of the nucleon from the projectile, leaving the residue c and the products $X = N + T$, which are not observed. Instead, the energy of the final state of the residue is measured.

One of the reasons why these reactions are of contemporary interest is because they offer the opportunity to study unstable, or radioactive, nuclei, such as, for instance, *halo* nuclei, which have one or few weakly bound neutrons (or protons) around the core.

The total cross section for such process contains two contributions: the stripping or inelastic contribution, where N reacts with and excites the target; and a diffractive contribution, where the dissociation of N from the projectile takes place through their two-body interactions with the target, both being elastically scattered while the target is left in its ground state. The cross sections for both processes must be taken into account and summed up in a reaction where only the final state of the residue is observed.

The actual reaction calculations are complex and require several steps and input items, such as the single-particle bound state wave functions for the relative motion of the $c + N$ system. For these preliminary tests, we will be using tools provided by Carlos Bertulani (see, for instance, Ref. [20]), to calculate the total knockout cross section for some selected processes.

In Table 3.1-3.2, the diffraction, stripping, and total cross sections are shown for the reaction $^{15}Be +^9 Be \rightarrow {}^{14}C + X$ at 40 Mev/nucleon and 250 MeV/nucleon, respectively. We stress again that these are exploratory tests, in that no adjustments of other components of the input or comparison with empirical information is being considered. In the Tables, "No Pauli Blocking" indicates that in-medium NN cross sections as shown in Figs. 3.5-3.6 are used, whereas "Pauli Blocking" signifies that the NN cross sections displayed in Figs. 3.7-3.8 are being employed. As to be expected, differences can be extremely large. Within each of the two categories, the differences between the LM and the DBHF entries reflect the model dependencies already observed when discussing those figures, see p. 15. Namely, at the lower energy, the LM values are smaller than those predicted by DBHF in absence of geometric blocking, whether the opposite is true when geometric blocking is applied. On the other hand, much less sensitivity to the description of medium effects, including geometric blocking, is observed at higher energies, see Table 3.2, as to be expected. This can be seen by moving horizontally through the Tables.

Notice that The differences between the entry "Pauli Blocking Free" and "Pauli Blocking DBHF" reflect the effect of using our microscopic in-medium NN cross sections in Eq. (2.1) rather than free-space cross sections.

	Reaction	σ	Free	LM	DBHF
No Pauli Blocking	$^9Be(^{15}C,^{14}C)$	σ_{dif}	19.14	9.853	15.47
		σ_{str}	49.14	39.10	42.87
		σ_{tot}	68.59	48.95	58.34
Pauli Blocking		σ_{dif}	4.998	3.918	3.844
		σ_{str}	32.99	33.34	30.85
		σ_{tot}	37.99	37.25	34.69

Table 3.1: Cross sections in mb at 40 MeV/nucleon for nucleon knockout. See text for details.

	Reaction	σ	Free	LM	DBHF
No Pauli Blocking	$^9Be(^{15}C,^{14}C)$	σ_{dif}	3.722	2.496	2.783
		σ_{str}	43.86	42.72	41.23
		σ_{tot}	47.58	45.21	44.02
Pauli Blocking		σ_{dif}	2.794	1.300	1.877
		σ_{str}	39.49	30.89	34.81
		σ_{tot}	42.28	32.19	36.69

Table 3.2: As in the previous Table, at 250 MeV/nucleon.

Chapter 4

Fitting procedure to reproduce the average in-medium NN cross sections

In order to utilize our predictions of in-medium effective NN cross sections in nucleus-nucleus reactions, a parametrization of the exact results is needed to reduce the calculation time required by the (five-fold) integral, Eq. (3.1). This is a non-trivial task, given that Eq. (3.1) depends on three variables.

First we will introduce two variables, $k_F = k_{F1} + k_{F2}$ and $k_G = |k_{F1} - k_{F2}|$, which govern different properties of the curve showed in Fig. 4.1. We attempt

$$\bar{\sigma}_{NN} = \sigma(k) \times e^{F(k,k_F)} \times e^{G(k,k_G)} \ , \tag{4.1}$$

with the restriction $G(k, 0) = 0$. In the equation above, $\sigma(k)$ is the cross section in free space, whereas $e^{F(k,k_F)} \times e^{G(k,k_G)}$ represent the geometrical Pauli blocking correction. Letting $k_G = 0$, we have

$$\bar{\sigma}_{NN}(k, k_F, 0) = \sigma(k) \times e^{F(k,k_F)} \ . \tag{4.2}$$

By using a bicubic interpolation, we can find the coefficients a_{ij} of the function $F(k, k_F) = \sum\limits_i \sum\limits_j a_{ij} k^i k_F^j$. In similar fashion, by fixing k_F, we can find the coefficient b_{ij} of function $G(k, k_G) = \sum\limits_i \sum\limits_{j \neq 0} b_{ij} k^i k_G^j$. The coefficients are given in Appendix A. We compare the interpolated values with the exact predictions in Fig. 4.2-4.3.

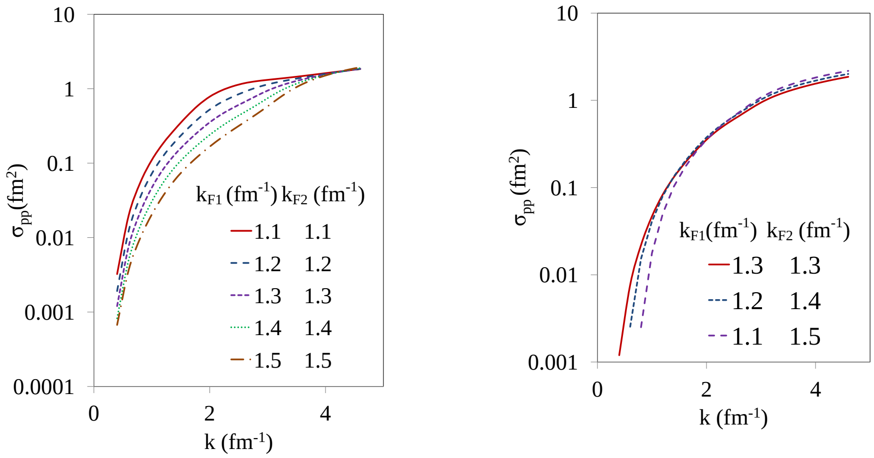

Figure 4.1: In-medium pp cross section calculated as in Eq. (3.1) for a variety of symmetric ($k_{F1} = k_{F2}$) and asymmetric ($k_{F1} \neq k_{F2}$) situations.

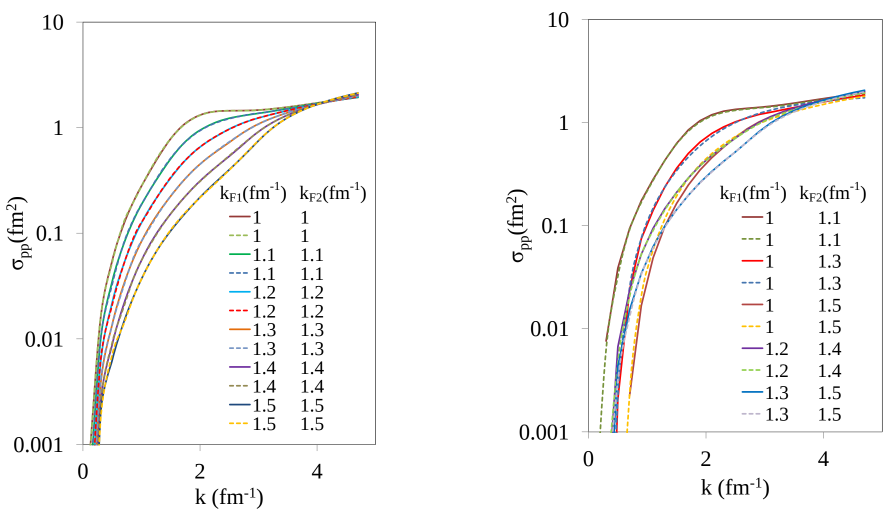

Figure 4.2: pp cross section in symmetric nuclear matter(left) and asymmetric nuclear matter(right). The dashed curves are interpolations.

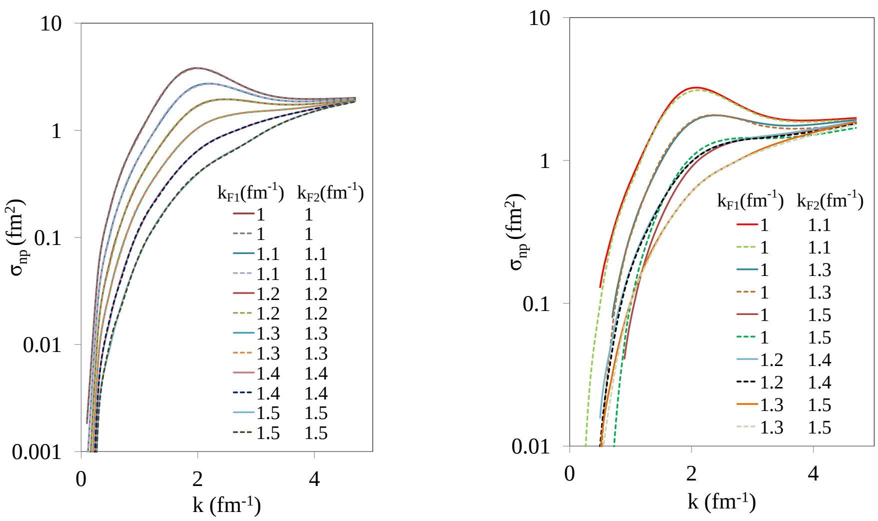

Figure 4.3: As in Fig. 4.2 for *np* scattering.

Chapter 5

Conclusions

Pauli blocking is perhaps the most important mechanism impacting the collision of two fermions in the medium. Its effect is to prevent scattering into already occupied states, as required by the Pauli Principle. Clearly, such mechanism impacts the scattering probability, and, in turn, the so-called in-medium cross section. Although the latter is not a directly observable quantity, it is an important component in nuclear reaction calculations.

In this thesis, we presented predictions of in-medium effective NN cross sections as a function of energy and density. As compared to a previous approach [15], they contain all important microscopic medium effects (implied by the Dirac-Brueckner-Hartree-Fock theory of nuclear matter), along with an improved description of Pauli blocking, which makes them more suitable for applications in nucleus-nucleus reactions.

First, we derived expressions for the appropriate geometric Pauli blocking factors to be included in the definition of the average in-medium NN cross section, where the *average* refers to all (allowed) momenta of two nucleons in the two colliding systems.

We then presented and discussed our predictions and explored model dependence by comparing with a popular set of predictions often used in the literature. Depending on the energy, model dependence can be large. In particular, we concentrated on the impact of including, or not, the geometric Pauli blocking effects as described in this work. Generally, the outcome of the integral which provides the averaged and Pauli-blocked in-medium cross section is found to be very sensitive to the energy dependence of the NN in-medium cross sections used in the integrand, particularly the high-energy behavior.

Computation of the averaged in-medium cross section involves five-fold integrals and thus is rather lengthy, particularly with regard to applications in nucleus-nucleus collisions, where an extremely large number of such cross sections needs to be available, as the calculation follows the density profiles of the two colliding nuclei. Therefore, we developed a convenient parametrization of our cross sections as a function of incident energy as well as nuclear densities. We hope that such tool will be helpful to reaction theorists.

Our future plans and work in progress include the application of these cross sections to reaction calculations with stable and unstable nuclei, along with a systematic comparison with the available database. Some preliminary calculations of total cross section in knockout reaction, which we conducted on an exploratory basis, suggest significant sensitivity to the input discussed in this thesis.

References

[1] H. Müther and A. Polls, Progress in Particle and Nuclear Physics **45**, 243 (2000).

[2] G.F. Bertsch and S. Das Gupta, Phys. Rep. **160**, 189 (1988).

[3] W. Cassing, W. Metag, U. Mosel, and K. Niita, Phys. Rep. **188**, 363 (1990).

[4] J. Aichelin, Phys. Rep. **202**, 235 (1991).

[5] C.M. Ko, Q. Li, and R.C. Wang, Phys. Rev. Lett. **59**, 1084 (1987).

[6] B. Blättel, V. Kock, W. Cassing, and U. Mosel, Phys. Rev. C **38**, 1767 (1988).

[7] H. Sorge, H. Stöcker, and W. Greiner, Ann. Phys. (N.Y.) **192**, 266 (1989).

[8] C.A. Bertulani and P. Danielewicz, "Introduction to Nuclear Reactions", IOP publishing, London (2004).

[9] R.J. Glauber, *Lectures on Theoretical Physics* Vol. I (Interscience, New York, 1959).

[10] V.R. Pandharipande and S.C. Pieper, Phys. Rev. C **45**, 791 (1992).

[11] D. Persram and C. Gale, Phys. Rev. C **65**, 064611 (2002).

[12] B.-A. Li and L.-W. Chen, Phys. Rev. C **72**, 064611 (2005).

[13] Cai Xiangzhou *et al.*, Phys. Rev. C **58**, 572 (1998).

[14] G.Q. Li and R. Machleidt, Phys. Rev. C **48**, 1702 (1993); **49**, 566 (1994).

[15] F. Sammarruca and P. Krastev, Phys. Rev. C **73**, 014001 (2006).

[16] M.S. Hussein, R.A. Rego, and C.A. Bertulani, Phys. Rep. **201**, 279 (1991).

[17] F. Sammarruca, Int. J. Mod. Phys. E **19**, 1259 (2010).

[18] F. Sammarruca, Eur. Phys. J. A **50**, 22 (2014).

[19] C. Bertulani, Rev. Bras. Fis. **16**, 380 (1986).

[20] C.A. Bertulani and P.G. Hansen, Phys. Rev. C **70**, 034609 (2004).

Appendix A: The interpolation

This appendix shows the parameterization of the average NN cross section. I used Matlab to do the interpolation and used Fortran to write the code to generate these results.

For the expressions given in Appendix A.1 and A.2, we introduce the following variables:

$$
\begin{aligned}
E_{lab} &= \frac{2h^2k^2}{m_n} \\
\gamma &= \frac{E_{lab}}{931.5} + 1 \\
\beta &= \sqrt{1 - \frac{1}{\gamma^2}}
\end{aligned}
\tag{5.1}
$$

and

$$
\begin{aligned}
E_{lab_2} &= \frac{h^2k^2}{2m_n} \\
\gamma_2 &= \frac{E_{lab_2}}{931.5} + 1 \\
\beta_2 &= \sqrt{1 - \frac{1}{\gamma_2^2}}
\end{aligned}
\tag{5.2}
$$

where $h = 197.326968$ and $m_n = 938.926$.

Appendix A.1. The interpolation of pp cross section

We define following functions:

$$\sigma_f(x) = c_1 + c_2 x^{-1} + c_3 x^{-1.75} + c_4 x^3 \tag{5.3}$$

Coefficients			
c_1	4.260406562946663	c_2	-4.861556441681672
c_3	2.373986813946191	c_4	0.701997337625813

$$F1(x,y) = \frac{p_0 y}{x^{.7} + p_1 y + p_2} + \frac{p_3 y^2 + p_4 y}{x^{.8} + p_5 y^2 + p_6 y + p_7} \tag{5.4}$$

Coefficients			
p_0	$-1.413748753823763E+002$	p_1	1.15415298629468
p_2	-0.469159506203645	p_3	12.087194211124997
p_4	$1.574913442839591E+002$	p_5	0.128404991481028
p_6	1.347501626170387	p_7	-0.465133973367518

$$LF1(x,y) = -\frac{p_{00} y^2 + p_{04} y}{x^{.73} + p_{01} y^2 + p_{02} y + p_{03}} + \frac{p_{05} y^2 + p_{06} y}{x + p_{09} y^2 + p_{07} y + p_{08}} \tag{5.5}$$

Coefficients			
p_{00}	43.389275582049407	p_{01}	-0.023951227203520
p_{02}	1.105998078953186	p_{03}	-0.179062693910055
p_{04}	9.306520451792869	p_{05}	80.006987731518180
p_{06}	5.866524331563402	p_{07}	2.616183254114989
p_{08}	-0.230830195370407	p_{09}	-0.187034542387308

$$LF2(x,y) = -\frac{p_{00}y^2 + p_{04}y}{x^{.73} + p_{01}y^2 + p_{02}y + p_{03}} + \frac{p_{05}y^2 + p_{06}y}{x + p_{09}y^2 + p_{07}y + p_{08}} \tag{5.6}$$

Coefficients			
p_{00}	-19.920588400569514	p_{01}	-1.945817823006394
p_{02}	3.729265023829234	p_{03}	-0.347042095839621
p_{04}	46.029928722162524	p_{05}	-35.811108998476634
p_{06}	85.328053558591492	p_{07}	7.002380637991235
p_{08}	0.408229490817838	p_{09}	-3.459569418866694

$$LG(x,y) = -\frac{p_{01}y^2 + p_{07}y}{p_{02}x^{p_{03}} + p_{04}y + p_{05}} + P_{06}y \tag{5.7}$$

Coefficients			
p_{01}	-17.038740312255214	p_{02}	-11.708710039502057
p_{03}	2.913953868414013	p_{04}	5.548569029195527
p_{05}	-0.946683373520670	p_{06}	-0.024217452930733
p_{07}	-1.956042942391835		

$$F2(x, y) = -\frac{p_{01}y^2 + p_{07}y}{p_{02}x^{p_{03}} + p_{04}y + p_{05}} + p_{06}y \tag{5.8}$$

Coefficients			
p_{01}	12.096517428606562	p_{02}	3.249135617903872
p_{03}	3.078924900132524	p_{04}	-0.244657926232791
p_{05}	0.118539186645611	p_{06}	-0.188403647445441
p_{07}	-0.083253429707312		

$$\begin{aligned} POLY1(x, y) = {} & p_{00} + p_{10}x + p_{01}y + p_{20}x^2 + p_{11}xy + p_{02}y^2 \\ & + p_{30}x^3 + p_{21}x^2y + p_{12}xy^2 + p_{03}y^3 + p_{40}x^4 \\ & + p_{31}x^3y + p_{22}x^2y^2 + p_{13}xy^3 + p_{04}y^4 + p_{50}x^5 \\ & + p_{41}x^4y + p_{32}x^3y^2 + p_{23}x^2y^3 + p_{14}xy^4 + p_{05}y^5 \end{aligned} \tag{5.9}$$

Coefficients			
p_{00}	26.333769952455828	p_{10}	13.451625025993231
p_{01}	-62.039245857071663	p_{20}	$-1.365229296659209E+002$
p_{11}	78.856778569613425	p_{02}	30.088101666700229
p_{30}	$1.892034702058778E+002$	p_{21}	-1.442476315007756
p_{12}	-50.146472881660941	p_{03}	-4.076862818268419
p_{40}	$-1.621392469810364E+002$	p_{31}	29.339809682507912
p_{22}	-10.261743310275275	p_{13}	15.959834385553462
p_{04}	-1.072522181779159	p_{50}	68.590575587794504
p_{41}	-35.095086655963414	p_{32}	14.501205538679383
p_{23}	-2.722078879896821	p_{14}	-1.337225677756676
p_{05}	0.237553992993964		

$$
\begin{aligned}
POLY2(x,y) = {} & p_{00} + p_{10}x + p_{01}y + p_{20}x^2 + p_{11}xy + p_{02}y^2 \\
& + p_{30}x^3 + p_{21}x^2y + p_{12}xy^2 + p_{03}y^3 + p_{40}x^4 \\
& + p_{31}x^3y + p_{22}x^2y^2 + p_{13}xy^3 + p_{04}y^4 + p_{50}x^5 \\
& + p_{41}x^4y + p_{32}x^3y^2 + p_{23}x^2y^3 + p_{14}xy^4 + p_{05}y^5
\end{aligned}
\tag{5.10}
$$

Coefficients			
p_{00}	41.942322634474600	p_{10}	16.554226016222600
p_{01}	$-1.018450793255731d+002$	p_{20}	-10.137921377513393
p_{11}	1.476324933362772	p_{02}	78.796407972449870
p_{30}	-1.212862244132186	p_{21}	9.005804013826475
p_{12}	-7.275789494180880	p_{03}	-29.513294431232829
p_{40}	0.985100800058586	p_{31}	-1.448454105725182
p_{22}	-1.421888774670954	p_{13}	2.404615930742827
p_{04}	5.412311857455272	p_{50}	-0.055582908502835
p_{41}	-0.213701227334434	p_{32}	0.628012466571997
p_{23}	-0.329149347271803	p_{14}	-0.094061445672775
p_{05}	-0.412357858063205		

$$\begin{aligned} POLY3(x,y) = {} & p_{00} + p_{10}x + p_{01}y + p_{20}x^2 + p_{11}xy + p_{02}y^2 \\ & + p_{30}x^3 + p_{21}x^2y + p_{12}xy^2 + p_{03}y^3 + p_{40}x^4 \\ & + p_{31}x^3y + p_{22}x^2y^2 + p_{13}xy^3 + p_{04}y^4 + p_{50}x^5 \\ & + p_{41}x^4y + p_{32}x^3y^2 + p_{23}x^2y^3 + p_{14}xy^4 + p_{05}y^5 \end{aligned} \tag{5.11}$$

Coefficients			
p_{00}	14.649808293288048	p_{10}	−13.856731230502055
p_{01}	−5.903851227851674	p_{20}	7.391090031566025
p_{11}	−3.264664322209852	p_{02}	8.043488376529455
p_{30}	−1.928288209134936	p_{21}	0.684394728979283
p_{12}	1.125578118352126	p_{03}	−4.412098977929499
p_{40}	0.207745946851701	p_{31}	0.272879406566840
p_{22}	−1.145703566520960	p_{13}	1.155972678353247
p_{04}	0.426708308572516	p_{50}	−0.007293260359370
p_{41}	−0.037299168442286	p_{32}	0.093986415682027
p_{23}	−0.025015144469598	p_{14}	−0.092509508027188
p_{05}	−0.005620957032146		

$$POLY4 = p_{00} + p_{10}x + p_{01}y + p_{20}x^2 + p_{11}xy + p_{02}y^2 \tag{5.12}$$

Coefficients			
p_{00}	0.131440589942482	p_{10}	0.159475522857123
p_{01}	−0.973306579880936	p_{20}	−0.034665819642854
p_{11}	0.140825174999997	p_{02}	0.081363287301587

The average in-medium pp cross section is given by:

$$\bar{\sigma}_{pp}(k, k_F, k_G) = \sigma(k) \times e^{F(k,k_F)} \times e^{G(k,k_G)} \tag{5.13}$$

where

<table>
<tr><td></td><td>$k_F < 1.5(fm^{-1})$</td><td>$1.5 \leq k_F \leq 3$</td><td>$3 < k_F$</td></tr>
<tr><td>$0 < k \leq 1$</td><td rowspan="2">$\sigma(k) = \sigma_f(\beta_2)$
$F(k, k_F) = LF1(k, k_F)$
$G(k, k_G) = LG(k, k_G)$</td><td>$\sigma(k) = \sigma_f(\beta)$
$F(k, k_F) = POLY1(k, k_F)$
$G(k, k_G) = F2(k, k_G)$</td><td rowspan="5">$\sigma(k) =$
$\sigma_f(\beta)$

$F(k, k_F) =$
$F1(k, k_F)$

$G(k, k_G) =$
$F2(k, k_G)$</td></tr>
<tr><td>$1 < k \leq 1.9$</td><td rowspan="2">$\sigma(k) = \sigma_f(\beta)$
$F(k, k_F) = POLY2(k, k_F)$
$G(k, k_G) = F2(k, k_G)$</td></tr>
<tr><td>$1.9 < k \leq 3$</td><td rowspan="3">$\sigma(k) = \sigma_f(\beta_2)$

$F(k, k_F) = LF2(k, k_F)$

$G(k, k_G) = LG(k, k_G)$</td></tr>
<tr><td>$3 < k \leq 4.3$</td><td>$\sigma(k) = \sigma_f(\beta)$
$F(k, k_F) = POLY3(k, k_F)$
$G(k, k_G) = F2(k, k_G)$</td></tr>
<tr><td>$4.3 < k$</td><td>$\sigma(k) = \sigma_f(\beta)$
$F(k, k_F) = POLY4(k, k_F)$
$G(k, k_G) = F2(k, k_G)$</td></tr>
</table>

Appendix A.2. The interpolation of np cross section

We define following functions:

$$\sigma_f = c_1 + c_2\beta^{-.8} + c_3\beta^{-.3} \tag{5.14}$$

Coefficients			
c_1	$1.653084178761176E+002$	c_2	74.251849686481776
c_3	$-2.354077526435100E+002$		

$$F1(x,y) = \frac{p_{00}y^2 + p_{01}y}{x^{1.4} + p_{02}y + p_{03}} + \frac{p_{05}y^2 + p_{06}y}{x^{2.8} + p_{09}y^2 + p_{07}y + p_{08}} \tag{5.15}$$

Coefficients			
p_{00}	3.853293143535447	p_{01}	-18.974693764773523
p_{02}	0.044303509832861	p_{03}	1.119295164994078
p_{04}		p_{05}	-30.845343065722332
p_{06}	$1.386867400182321E+002$	p_{07}	-14.717626152511599
p_{08}	28.070469478383458	p_{09}	4.806760155370110

$$F2(x,y) = -\frac{p_{01}y^2 + p_{07}y}{p_{02}x^{p_{03}} + p_{04}y + p_{05}} + p_{06}y \tag{5.16}$$

Coefficients			
p_{01}	$6.657898733390806E-004$	p_{02}	$1.986304380452931E-004$
p_{03}	3.056423165151889	p_{04}	$-1.989016700886466E-005$
p_{05}	$9.624733085105337E-006$	p_{06}	-0.237962025768914
p_{07}	$3.325923525508616E-005$		

$$LDF1(x,y) = -\frac{p_{00}y^2 + p_{04}y}{x^{.73} + p_{01}y^2 + p_{02}y + p_{03}} + \frac{p_{05}y^2 + p_{06}y}{x^{1.2} + p_{09}y^2 + p_{07}y + p_{08}} \tag{5.17}$$

Coefficients			
p_{00}	-4.799656344645658	p_{01}	-0.184111965270962
p_{02}	0.903693199612923	p_{03}	0.045533467610811
p_{04}	29.868464900022744	p_{05}	19.339115527338894
p_{06}	37.597464689950584	p_{07}	1.893770274897013
p_{08}	0.313399071544287	p_{09}	1.120323361203023

$$\begin{aligned} LDF2 = {} & p_{10}x + p_{01}y + p_{20}x^2 + p_{11}xy + p_{02}y^2 + p_{30}x^3 \\ & + p_{21}x^2y + p_{12}xy^2 + p_{03}y^3 + p_{40}x^4 + p_{31}x^3y \\ & + p_{22}x^2y^2 + p_{13}xy^3 + p_{04}y^4 + p_{50}x^5 + p_{41}x4y \\ & + p_{32}x^3y^2 + p_{23}x^2y^3 + p_{14}xy^4 + p_{05}y^5 \end{aligned} \tag{5.18}$$

Coefficients			
p_{10}	0.475370305238253	p_{01}	0.121715624174776
p_{20}	−1.176533243068061	p_{11}	0.162589252084993
p_{02}	−1.233856984064353	p_{30}	0.732067700034925
p_{21}	−0.195167009728208	p_{12}	0.886689353837032
p_{03}	0.185524480756406	p_{40}	−0.166166684041222
p_{31}	0.061673129997645	p_{22}	−0.246310307260954
p_{13}	0.006977256446957	p_{04}	−0.139592101125880
p_{50}	0.012667859638694	p_{41}	−0.006123675478641
p_{32}	0.023733271811769	p_{23}	−0.006776845194641
p_{14}	0.016130830971479	p_{05}	0.019593934847803

$$LDF3 = p_{10}x + p_{01}y + p_{20}x^2 + p_{11}xy + p_{02}y^2 \tag{5.19}$$

Coefficients			
p_{10}	0.475370305238253	p_{01}	0.121715624174776
p_{20}	−1.176533243068061	p_{11}	0.162589252084993
p_{02}	−1.233856984064353	p_{30}	0.732067700034925
p_{21}	−0.195167009728208	p_{12}	0.886689353837032
p_{03}	0.185524480756406	p_{40}	−0.166166684041222
p_{31}	0.061673129997645	p_{22}	−0.246310307260954
p_{13}	0.006977256446957	p_{04}	−0.139592101125880
p_{50}	0.012667859638694	p_{41}	−0.006123675478641
p_{32}	0.023733271811769	p_{23}	−0.006776845194641
p_{14}	0.016130830971479	p_{05}	0.019593934847803

$$LDG(x,y) = -\frac{p_{01}y^2 + p_{07}y}{p_{02}x^{p_{03}} + p_{04}y + p_{05}} + P_{06}y \tag{5.20}$$

Coefficients			
p_{01}	-0.025522993889389	p_{02}	-0.010053091405470
p_{03}	4.246210775015689	p_{04}	$-8.750342973161255E-005$
p_{05}	$-3.183281577044425E-004$	p_{06}	-0.112849736069339
p_{07}	$9.433816459771692E-004$		

$$\begin{aligned} POLY1(x,y) = {} & p_{00} + p_{10}x + p_{01}y + p_{20}x^2 + p_{11}xy + p_{02}y^2 \\ & + p_{30}x^3 + p_{21}x^2y + p_{12}xy^2 + p_{03}y^3 + p_{40}x^4 \\ & + p_{31}x^3y + p_{22}x^2y^2 + p_{13}xy^3 + p_{04}y^4 + p_{50}x^5 \\ & + p_{41}x^4y + p_{32}x^3y^2 + p_{23}x^2y^3 + p_{14}xy^4 + p_{05}y^5 \end{aligned} \tag{5.21}$$

Coefficients			
p_{00}	$1.686882067050742E+002$	p_{10}	36.397760671117688
p_{01}	$-3.708800260899917E+002$	p_{20}	$-1.121542280376210E+002$
p_{11}	20.486883437642238	p_{02}	$3.011938949047040E+002$
p_{30}	$1.646133848210874E+002$	p_{21}	-6.356936584451566
p_{12}	-11.457524468421022	p_{03}	$-1.223650720326252E+002$
p_{40}	$-1.495320405450191E+002$	p_{31}	36.181983418519479
p_{22}	-12.357887684112296	p_{13}	5.681702618960386
p_{04}	24.469400087738510	p_{50}	61.507746186777538
p_{41}	-29.982610174873340	p_{32}	10.114956688165400
p_{23}	-1.108357099460476	p_{14}	-0.497015545521594
p_{05}	-1.941273355107718		

$$\begin{aligned} POLY2(x,y) = {} & p_{00} + p_{10}x + p_{01}y + p_{20}x^2 + p_{11}xy + p_{02}y^2 \\ & + p_{30}x^3 + p_{21}x^2y + p_{12}xy^2 + p_{03}y^3 + p_{40}x^4 \\ & + p_{31}x^3y + p_{22}x^2y^2 + p_{13}xy^3 + p_{04}y^4 + p_{50}x^5 \\ & + p_{41}x^4y + p_{32}x^3y^2 + p_{23}x^2y^3 + p_{14}xy^4 + p_{05}y^5 \end{aligned} \tag{5.22}$$

Coefficients			
p_{00}	$1.029411180213104E+002$	p_{10}	4.736442921490927
p_{01}	$-2.191998233542346E+002$	p_{20}	0.957130691886176
p_{11}	5.748899925334489	p_{02}	$1.732810609272639E+002$
p_{30}	-9.738375207842861	p_{21}	15.913294311049897
p_{12}	-14.723009456313964	p_{03}	-66.335070348731080
p_{40}	3.635629122105692	p_{31}	-4.045931411532593
p_{22}	-0.735476092785353	p_{13}	3.771014568306572
p_{04}	12.697218276192412	p_{50}	-0.316443193467803
p_{41}	-0.049209831187591	p_{32}	0.838672465866954
p_{23}	-0.598583977202799	p_{14}	-0.098737241105921
p_{05}	-1.009411200313251		

$$
\begin{aligned}
POLY3(x,y) = {} & p_{00} + p_{10}x + p_{01}y + p_{20}x^2 + p_{11}xy + p_{02}y^2 \\
& + p_{30}x^3 + p_{21}x^2y + p_{12}xy^2 + p_{03}y^3 + p_{40}x^4 \\
& + p_{31}x^3y + p_{22}x^2y^2 + p_{13}xy^3 + p_{04}y^4 + p_{50}x^5 \\
& + p_{41}x^4y + p_{32}x^3y^2 + p_{23}x^2y^3 + p_{14}xy^4 + p_{05}y^5 \qquad (5.23)
\end{aligned}
$$

Coefficients			
p_{00}	29.149282824659615	p_{10}	−11.993764892488336
p_{01}	−35.835765644123292	p_{20}	3.032577431442097
p_{11}	3.789440062832123	p_{02}	30.041340986392068
p_{30}	0.224537514189215	p_{21}	−2.852352852257145
p_{12}	1.195767493190272	p_{03}	−13.844357893303632
p_{40}	−0.179373217311273	p_{31}	0.758591430358696
p_{22}	−0.714648053568228	p_{13}	0.831171078074083
p_{04}	2.459725374668622	p_{50}	0.012947686442894
p_{41}	−0.028070610857844	p_{32}	−0.036704204902122
p_{23}	0.106218897776375	p_{14}	−0.159404133127777
p_{05}	−0.148675942384911		

$$POLY4 = p_{00} + p_{10}x + p_{01}y + p_{20}x^2 + p_{11}xy + p_{02}y^2 \tag{5.24}$$

Coefficients			
p_{00}	3.133984061641012	p_{10}	−0.918089599571409
p_{01}	−1.309430160008916	p_{20}	0.039871547321427
p_{11}	0.242217505267856	p_{02}	0.018965152008927

The average in-medium np cross section is given by:

$$\bar{\sigma}_{np}(k, k_F, k_G) = \sigma(k) \times e^{F(k,k_F)} \times e^{G(k,k_G)} \tag{5.25}$$

where

<table>
<tr><td></td><td>$k_F < 1.6(fm^{-1})$</td><td>$1.6 \leq k_F \leq 3$</td><td>$3 < k_F$</td></tr>
<tr><td>$0 < k \leq 1$</td><td rowspan="2">$\sigma(k) = \sigma_f(\beta_2)$
$F(k, k_F) = LDF1(k, k_F)$
$G(k, k_G) = LDG(k, k_G)$</td><td>$\sigma(k) = \sigma_f(\beta)$
$F(k, k_F) = POLY1(k, k_F)$
$G(k, k_G) = F2(k, k_G)$</td><td rowspan="5">$\sigma(k) = \sigma_f(\beta)$
$F(k, k_F) = F1(k, k_F)$
$G(k, k_G) = F2(k, k_G)$</td></tr>
<tr><td>$1 < k \leq 1.9$</td><td rowspan="2">$\sigma(k) = \sigma_f(\beta)$
$F(k, k_F) = POLY2(k, k_F)$
$G(k, k_G) = F2(k, k_G)$</td></tr>
<tr><td>$1.9 < k \leq 3$</td><td rowspan="2">$\sigma(k) = \sigma_f(\beta_2)$
$F(k, k_F) = LDF2(k, k_F)$
$G(k, k_G) = LDG(k, k_G)$</td></tr>
<tr><td>$3 < k \leq 4.3$</td><td>$\sigma(k) = \sigma_f(\beta)$
$F(k, k_F) = POLY3(k, k_F)$
$G(k, k_G) = F2(k, k_G)$</td></tr>
<tr><td>$4.3 < k$</td><td>$\sigma(k) = \sigma_f(\beta_2)$
$F(k, k_F) = LDF3(k, k_F)$
$G(k, k_G) = LDG(k, k_G)$</td><td>$\sigma(k) = \sigma_f(\beta)$
$F(k, k_F) = POLY4(k, k_F)$
$G(k, k_G) = F2(k, k_G)$</td></tr>
</table>